Chemical Engineering Communications

ISSN: 0098-6445 (Print) 1563-5201 (Online) Journal homepage: www.tandfonline.com/journals/gcec20

COMBINED CONDUCTION-MIXED CONVECTION-SURFACE RADIATION FROM A UNIFORMLY HEATED VERTICAL PLATE

S. M. Sawant & C. Gururaja Rao

To cite this article: S. M. Sawant & C. Gururaja Rao (2010) COMBINED CONDUCTION-MIXED CONVECTION-SURFACE RADIATION FROM A UNIFORMLY HEATED VERTICAL PLATE, Chemical Engineering Communications, 197:6, 881-899, DOI: 10.1080/00986440903359053

To link to this article: https://doi.org/10.1080/00986440903359053

Published online: 21 Jan 2010.

Chem. Eng. Comm., 197:881–899, 2010

ISSN: 0098-6445 print/1563-5201 online
DOI: 10.1080/00986440903359053

Taylor & Francis
Taylor & Francis Group

Combined Conduction-Mixed Convection-Surface Radiation from a Uniformly Heated Vertical Plate

S. M. SAWANT AND C. GURURAJA RAO

Department of Mechanical Engineering, National Institute of Technology, [Deemed University], Warangal, India

The present article reports the results of a numerical study on combined conduction-mixed convection-surface radiation from a vertical plate with uniform internal heat generation. The study considers the governing fluid flow and heat transfer equations without boundary layer approximations. Air is taken to be the cooling medium. Stream function-vorticity formulation, coupled with finite volume method, is used to solve the problem. A computer code has been written for the purpose, and results are validated with available experimental and analytical results for asymptotic limiting cases. In addition to making comprehensive parametric studies, useful correlations for evaluating the nondimensional maximum and average temperatures of the plate and mean friction coefficient are deduced based on a large set of data generated from the code.

Keywords Conduction; Mixed convection; Surface radiation; Uniformly heated vertical plate

Introduction

The geometry of a flat plate involved in fluid flow and heat transfer is not new in the literature. Starting with Blasius (1908), who gave the solution for fluid flow pertaining to laminar forced convection from an isothermal flat plate, there have been several analytical and numerical as well as experimental works addressing the above geometry. Pohlhausen (1921) provided a solution to heat transfer during forced convection laminar flow and Ostrach (1953) reported the results of both fluid flow and heat transfer for laminar free convection flow past the above geometry. With regard to mixed convection, Sparrow and Gregg (1959), Kliegel (1959), Lloyd and Sparrow (1970), Wilks (1973), and Oosthuizen and Hart (1973) are among those who have provided noteworthy contributions.

Ramachandran et al. (1985) documented experimental measurements as well as numerical predictions of laminar mixed (forced and free) convection involving the flow of air adjacent to an isothermally heated vertical flat surface. Chen et al. (1986) deduced several correlations for the local and average Nusselt numbers for laminar mixed convection flows along isothermal vertical, inclined, and horizontal flat plates valid for the entire mixed convection regime and for a wide range of Prandtl numbers

Address correspondence to C. Gururaja Rao, Department of Mechanical Engineering, National Institute of Technology, Warangal – 506 004 (A.P.), India. E-mail: cgr_gcr@yahoo.co.in

($0.1 < Pr < 100$). The correlations that they have given are based on the numerical results obtained using the well-known boundary layer approximations. A detailed review of the numerical analysis of laminar mixed convection in external flows using the boundary layer approximations has been provided by Chen (1995). He arrived at several correlations useful for the local and average Nusselt numbers that are present in this kind of problem. Gururaja Rao et al. (2000) made a numerical investigation into laminar mixed convection from an isothermal vertical flat plate and deduced correlations for the calculation of average Nusselt number (i) for the range of parameters used by Chen et al. (1986) and (ii) for low Prandtl number fluids at low Grashof numbers.

Several practical situations, like cooling of electronic equipment and devices, solar collectors, and gas-cooled nuclear reactors, to name a few, involve multiple modes of heat transfer. Zinnes (1970), Lee and Yovanovich (1989), Tewari and Jaluria (1990), Gorski and Plumb (1992), Kishinami et al. (1995), Merkin and Pop (1996), Wang et al. (1997), Kimura et al. (1998), and Mendez and Trevino (2000) reported some prominent results in this context. Gururaja Rao et al. (2001) solved, numerically, the problem of two-dimensional steady incompressible conjugate laminar mixed convection with surface radiation from a vertical plate with a flush-mounted discrete heat source. Gururaja Rao (2004) investigated buoyancy-aided conjugate mixed convection with surface radiation from a vertical electronic board equipped with a traversable flush-mounted discrete heat source. Recently, Jahangeer et al. (2007) dealt with the conjugate heat transfer problem concerning the rectangular fuel element of a nuclear reactor dissipating heat into an upward moving liquid sodium stream using the boundary layer approximations.

A detailed survey of literature on mixed convection and multimode heat transfer pertaining to the geometry of a vertical plate brings out the following points. No available study appears to address, in requisite detail, the interactive effect of surface radiation on conjugate mixed convection (mixed convection coupled with conduction) from a vertical plate with internal heat generation. There are no correlations available that help in calculating the maximum and average temperatures of the vertical plate for the above kind of situation. Another important observation that has been made is that no correlations are reported to compute the mean friction coefficient that are valid in the entire mixed convection regime and for varying operating conditions for this kind of geometry. It is known that the mean friction coefficient helps in calculating the pumping power requirement to sustain the flow.

In view of the above, an attempt has been made in the present study to numerically solve the problem of conjugate, laminar, mixed convection with surface radiation from a uniformly heated vertical plate. Possible applications for this kind of geometry are electronic boards and slab-shaped nuclear fuel elements. The governing fluid flow and heat transfer equations were solved using stream function-vorticity formulation coupled with the finite volume method. A computer code was written for the purpose and a comprehensive parametric study was made, which ends with correlations for pertinent parameters concerning the problem.

Mathematical Formulation

Figure 1(a) shows the schematic of the problem geometry chosen for the present study along with the system of coordinates. It consists of a vertical plate of height L and thickness t. The thermal conductivity of the plate is k_s and surface emissivity is ε. The plate has a uniform volumetric heat generation at the rate of q_v W/m^3.

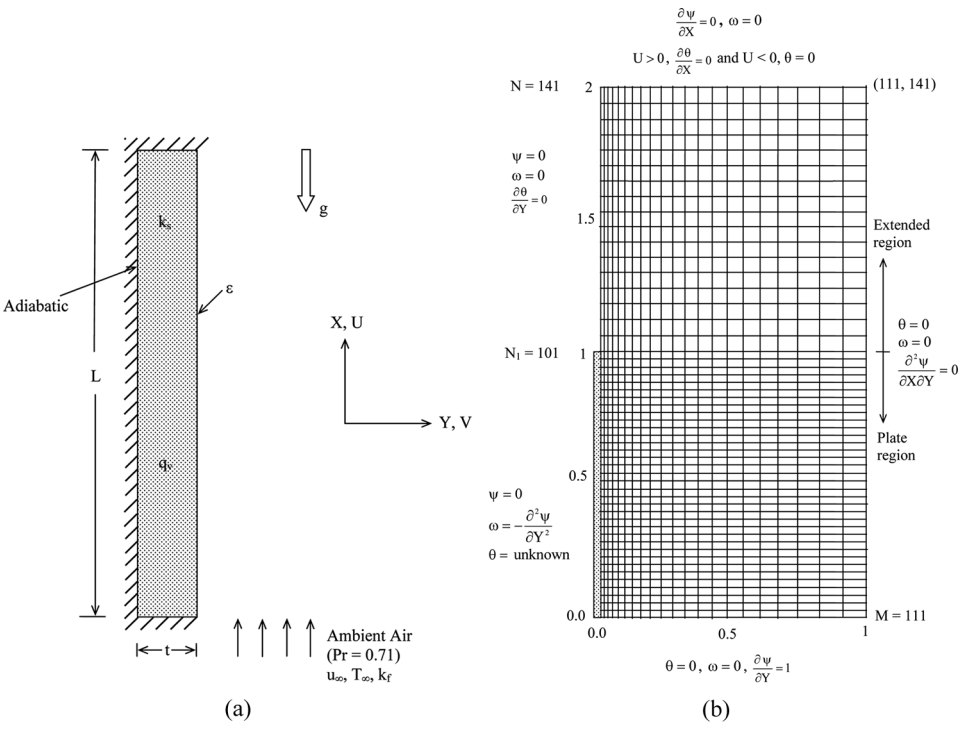

Figure 1. (a) Schematic of the problem geometry considered for study along with system of coordinates. (b) Discretized computational domain along with boundary conditions considered in the present study.

The bottom, left, and top surfaces of the plate are adiabatic. The plate is considerably thin in comparison to its height [t << L], implying axial conduction alone along the plate. The heat generated in the plate is conducted along the plate and is subsequently dissipated by mixed convection and radiation from the right surface of the plate. The basic equations of fluid flow and heat transfer are the continuity equation, the two momentum equations, and the energy equation that are available in references like Bejan (1984). The fluid (air) is assumed to be of constant thermo-physical properties with only density in the body force term of the x-momentum equation varying as per the Boussinesq approximation. The governing equations in primitive variable form are transformed into the vorticity-stream function form and later normalized using the nondimensional parameters defined in nomenclature. The above gives rise to the nondimensional set of governing equations as:

$$\mathrm{U}\frac{\partial\omega}{\partial\mathrm{X}} + \mathrm{V}\frac{\partial\omega}{\partial\mathrm{Y}} = -\mathrm{Ri}_\mathrm{L}^*\frac{\partial\theta}{\partial\mathrm{Y}} + \frac{1}{\mathrm{Re}_\mathrm{L}}\left(\frac{\partial^2\omega}{\partial\mathrm{X}^2} + \frac{\partial^2\omega}{\partial\mathrm{Y}^2}\right) \tag{1}$$

$$\frac{\partial^2\psi}{\partial\mathrm{X}^2} + \frac{\partial^2\psi}{\partial\mathrm{Y}^2} = -\omega \tag{2}$$

$$\mathrm{U}\frac{\partial\theta}{\partial\mathrm{X}} + \mathrm{V}\frac{\partial\theta}{\partial\mathrm{Y}} = \frac{1}{\mathrm{Pe}_\mathrm{L}}\left(\frac{\partial^2\theta}{\partial\mathrm{X}^2} + \frac{\partial^2\theta}{\partial\mathrm{Y}^2}\right) \tag{3}$$

In Equation (1) above, Ri_L^* is the modified Richardson number (or the modified buoyancy parameter) that gives the ratio of modified Grashof number (Gr_L^*) to square of the Reynolds number (Re_L). It serves as the governing mixed convection parameter, and it physically indicates the dominance of the buoyancy forces in comparison to the inertia forces and vice versa. It helps in demarking the entire mixed convection regime into three sub-regimes: forced convection dominant regime, pure mixed convection regime, and free convection dominant regime.

The normalized governing equations given above are elliptic and thus warrant specification of boundary conditions on all four boundaries. In the present problem, the plate forms the solid boundary and the remaining three boundaries are open (or free) boundaries. An extended computational domain is considered based on some initial studies performed taking different heights and widths for the computational domain. The optimum values of the height (H) and the width (W) turned out to be 2L and L, respectively. With regard to discretization of the computational domain, it is ensured that there are closely packed grids along the plate between its leading and trailing edges, while in the extended domain in the vertical direction, it would suffice to have coarser grids. In the horizontal direction, near the surface of the plate, it is mandatory to have finer grids as the velocity and temperature gradients would be steeper here. In view of the above, semi-cosine grids are employed in the horizontal direction. With regard to the vertical direction, finer uniform grids are used along the plate, while coarser uniform grids are taken beyond the trailing edge of the plate. Figure 1(b) shows the computational domain along with the boundary conditions that have been considered in the present problem.

With regard to the boundary conditions, along the bottom boundary, $\frac{\partial\psi}{\partial Y}=1$, $\omega=0$, and $\theta=0$ are used. In view of the extended domain chosen, the left boundary contains two parts, the first part, which is the plate itself, and the second part, which pertains to the extended length. Thus, the left boundary has a solid boundary accompanied by open boundary in it. As far as the plate portion is concerned, $\psi=0$ and $\omega=-\frac{\partial^2\psi}{\partial Y^2}$ have been used for stream function and vorticity. The governing equation for temperature distribution along the plate has been derived by appropriate energy balance between the heat generated, conducted, convected, and radiated. For example, for an element of the plate other than the top and bottom adiabatic ends, energy balance results in:

$$q_{cond,x,in} + q_v \Delta x_h t = q_{cond,x,out} + q_{conv} + q_{rad} \tag{4}$$

Expanding the first term on the right side of the above equation using Taylor's series and substituting for various terms appropriately, one gets:

$$k_s t \frac{\partial^2 T}{\partial x^2} + k_f \left(\frac{\partial T}{\partial y}\right)_{y=0} + q_v t - \sigma\varepsilon(T^4 - T_{\infty^4}) = 0 \tag{5}$$

Nondimensionalization of the above equation and simplification gives the governing equation for temperature distribution along the plate other than its bottom and top adiabatic ends as:

$$\frac{\partial^2\theta}{\partial X^2} + \gamma\left(\frac{\partial\theta}{\partial Y}\right)_{Y=0} + A_{r1} - \varepsilon\gamma N_{RF}\left[\left(\frac{T}{T_\infty}\right)^4 - 1\right] = 0 \tag{6}$$

Here, γ is the thermal conductance parameter, N_{RF} is the radiation-flow interaction parameter, and A_{r1} is the nondimensional geometric ratio, they are defined as in the nomenclature. For the bottom adiabatic end of the plate, an energy balance made on the element pertinent to it results in:

$$q_v\left(\frac{\Delta x_h}{2}\right)t = q_{cond,x,out} + q_{conv} + q_{rad} \tag{7}$$

Substitution of relevant expressions for various terms, normalization, and subsequent simplification of the above equation leads to:

$$\frac{\partial\theta}{\partial X} + \gamma\frac{\Delta X_h}{2}\left(\frac{\partial\theta}{\partial Y}\right)_{Y=0} + A_{r1}\frac{\Delta X_h}{2} - \varepsilon\gamma N_{RF}\frac{\Delta X_h}{2}\left[\left(\frac{T}{T_\infty}\right)^4 - 1\right] = 0 \tag{8}$$

The governing equation for the temperature of the top adiabatic end of the plate could also be obtained by relevant energy balance on the concerned element and it is:

$$\frac{\partial\theta}{\partial X} - \gamma\frac{\Delta X_h}{2}\left(\frac{\partial\theta}{\partial Y}\right)_{Y=0} - A_{r1}\frac{\Delta X_h}{2} + \varepsilon\gamma N_{RF}\frac{\Delta X_h}{2}\left[\left(\frac{T}{T_\infty}\right)^4 - 1\right] = 0 \tag{9}$$

Along the extended section of the left boundary, $\psi = 0$, $\omega = 0$, and $\frac{\partial\theta}{\partial Y} = 0$ are used for stream function, vorticity, and temperature. Along the top boundary, the stream function (ψ) satisfies the fully developed condition, i.e., $\frac{\partial\psi}{\partial X} = 0$, while for vorticity, the irrotationality condition, $\omega = 0$, is used. For nondimensional temperature (θ), two possibilities are considered: (i) when the vertical velocity (U) is positive, the fully developed condition, given by $\frac{\partial\theta}{\partial X} = 0$, is used and (ii) when the vertical velocity (U) is negative, indicating an incoming flow, $\theta = 0$ is used since the fluid coming in is assumed to enter at the free stream temperature (T_∞). Gururaja Rao et al. (2000, 2001) proposed the condition for stream function (ψ) along the right open boundary of the computational domain as: $\frac{\partial^2\psi}{\partial X\partial Y} = 0$ and the same is used here also. For ω, since the right boundary is at a distance equal to the plate height from the surface of the plate, it is appropriate to assume irrotationality ($\omega = 0$). The nondimensional temperature (θ) is taken equal to zero along the right boundary owing to the above reason itself.

Method of Solution

The normalized governing equations as obtained above are nonlinear partial differential equations. These equations are transformed into finite difference equations using the finite-volume method of Gosman et al. (1969), and the algebraic equations thus obtained are solved using the Gauss-Seidel iterative procedure. Under-relaxation is imposed over stream function (ψ) and vorticity (ω) with a relaxation parameter of 0.5 identified for the purpose, and for temperature (θ), full relaxation (relaxation parameter = 1) was found appropriate. Based on some initial numerical experiments, the appropriate convergence criteria on ψ, ω, and θ have been found to be, respectively, 1×10^{-4}, 5×10^{-4}, and 1×10^{-4}. The Lagrangian three-point formula has been used for calculating various derivatives present in different boundary conditions and Simpson's 1/3 rule is used for performing integrations that are necessary in the calculations.

A computer code in C was written to solve the problem. All the calculations have been performed considering air to be the cooling medium. The height of the plate (L) has been taken to be 20 cm, which is the typical height practically employed for printed circuit boards. The plate thickness (t) is taken to be 1.5 mm. The volumetric heat generation (q_v) within the vertical plate was varied between 10^5 and $10^6\,W/m^3$ since these values of q_v gave rise to peak plate temperature (T_{max}) hovering around 150°C. Values of q_v beyond $10^6\,W/m^3$ were not considered since they resulted in larger values of T_{max} that are not acceptable in electronic cooling applications. The thermal conductivity of the plate (k_s) was varied between 0.25 and 1 W/m K because electronic boards, which form a possible application to the present problem, are typically made of materials of thermal conductivity of the order of unity (epoxy glass with $k_s = 0.26\,W/m\,K$). The surface emissivity (ε) of the plate was varied between 0.05 and 0.85. Here, $\varepsilon = 0.05$ pertains to a highly polished aluminum foil, while $\varepsilon = 0.85$ belongs to black paint. However, the values of ε equal to 0 and 1 have also been used while discussing the exclusive effect of surface radiation on the results. In order to determine the appropriate range for modified Richardson number (Ri_L^*), the present problem has been solved for different values of Ri_L^*: 250, 25, 1, 0.25, 0.1, and 0.05. No appreciable change was observed in θ_{max} between $Ri_L^* = 250$ and 25. Likewise, there was very little change in θ_{max} as Ri_L^* is decreased from 0.1 to 0.05. Thus, it has been decided to restrict Ri_L^* to between 25 and 0.1.

Results and Discussion

Grid Sensitivity Analysis

Before taking up the parametric studies related to the present problem, a detailed grid sensitivity analysis was made to arrive at the optimum grid size needed to discretize the computational domain. The analysis was performed for a fixed set of parameters: $q_v = 10^6\,W/m^3$, $k_s = 0.25\,W/m\,K$, and $\varepsilon = 0.45$. The objective of analysis is to identify the optimum values for (i) the number of grids in the horizontal direction (M), (ii) the number of grids in the vertical direction (N), and (iii) the number of grids along the plate (N_1). Thus, there are three stages in the present grid sensitivity analysis. Further, since the flow regime can be (i) free convection dominant regime, (ii) mixed convection regime, and (iii) forced convection dominant regime, it is imperative to do the analysis for all three regimes of convection in each stage. To do this, three typical values of Ri_L^*, 25, 1, and 0.1, were chosen with $Ri_L^* = 25$ implying free convection dominant regime, $Ri_L^* = 1$ meaning pure mixed convection, and $Ri_L^* = 0.1$ indicating forced convection dominant regime. The sensitivity of the peak plate temperature and the mean friction coefficient with reference to the varying grid size has been checked. The best possible values for the number of grids in the vertical direction (N), along the plate (N_1), and across the plate (M) turned out to be, 141, 101, and 111, respectively, and these values were used for obtaining all the results of the present study.

Testing the Results for Mass and Energy Balance

The results of the present problem have been checked for conservation of mass and energy. In order to do this, a comparison is made between (i) the mass inflow rate and the mass outflow rate for mass conservation and (ii) the total rate of heat

generation in the plate and the net rate of heat dissipation by mixed convection and radiation from the plate for energy conservation. A typical case comprising $q_v = 10^6\,W/m^3$, $k_s = 0.25\,W/m\,K$, $\varepsilon = 0.45$, and $Ri_L^* = 1$ has been considered for the above check. The mass balance and the energy balance have been found to be satisfactory with the maximum deviation, lying within $\pm 0.05\%$ and $\pm 0.31\%$, respectively. Subsequently, calculations were made for various other values of Ri_L^* in the range $0.1 \leq Ri_L^* \leq 25$ with other parameters also considered appropriately. Similar observations as above have been made with respect to all those cases also.

Validation of Results

It has been mentioned already that a computer code in C was written to solve the present problem. The validation of the fluid flow and heat transfer results pertaining to the problem was made with the available analytical, experimental, and numerical results. In order to do this, results were obtained from the code for the limiting case where the vertical plate does not have heat generation in it and is instead maintained at a prescribed uniform temperature (T_w) greater than the free stream temperature (T_∞) of air. When this is done, ΔT_{ref} will no longer be equal to $(\frac{q_{vLt}}{k_s})$ and would become equal to the known temperature difference $(T_w - T_\infty)$. Now, in the place of Ri_L^* (modified Richardson number) one would get Ri_L (Richardson number), which is equal to $[\frac{g\beta(T_w - T_\infty)L}{u_\infty^2}]$. The modified Grashof number (Gr_L^*) would then become Grashof number (Gr_L), which is related to Ri_L by the equation $Ri_L = \frac{Gr_L}{Re_L^2}$. In the light of the above changes in the limiting case considered, it has been noticed that the asymptotic free and forced convection limits for Ri_L become, respectively, 10^5 and 10^{-5}, with $Ri_L = 1$ indicating pure mixed convection. Subsequently, verification of results for the asymptotic forced convection limit was made against the well-known exact solutions of Blasius (1908) and Pohlhausen (1921). For the results of the asymptotic free convection limit, the exact solution of Ostrach (1953) has been used. Further, the results belonging to the mixed convection regime were checked by means of comparison with the experimental results of Ramachandran et al. (1985), the numerical results of Chen et al. (1986), and the numerical results of Gururaja Rao et al. (2000). The values of $Ri_L = 0.01$, 1, and 100, respectively, indicating the asymptotic forced convection, pure mixed convection, and asymptotic free convection regimes, have been chosen as far as the work of Chen et al. (1986) is concerned. The corresponding values as far as the work of Gururaja Rao et al. (2000) is concerned have been chosen to be $Ri_L = 10^{-5}$, 1, and 10^5, respectively. The parameter considered for comparison was average Nusselt number. The maximum deviation with reference to Chen et al. has been noticed to be $\pm 2.1\%$ and that with reference to Gururaja Rao et al. turned out to be $\pm 1.7\%$. In addition to the above, the calculation for mean friction coefficient is validated with respect to that of Blasius (1908) for the asymptotic forced convection case.

Variation of Nondimensional Local Plate Temperature with Other Parameters

Figure 2 shows the nondimensional local plate temperature profiles plotted for different surface emissivities in various regimes of convection. It may be noticed that Figures 2(a), 2(b), and 2(c), respectively, refer to forced convection dominant regime ($Ri_L^* = 0.1$), pure mixed convection ($Ri_L^* = 1$), and free convection dominant regime

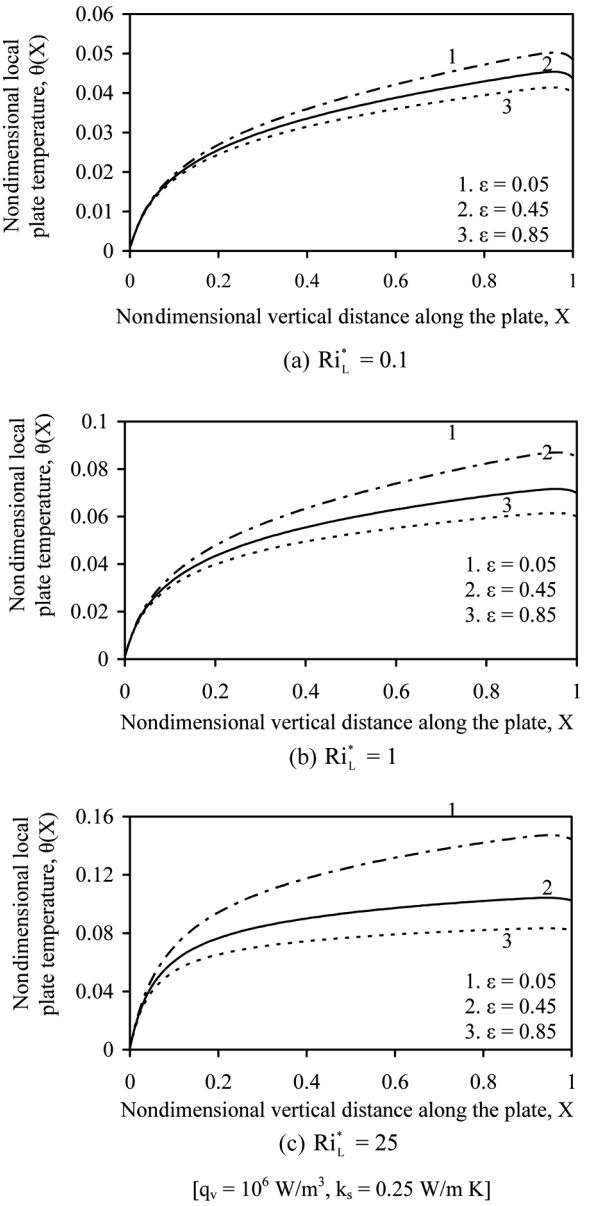

Figure 2. Nondimensional local plate temperature profiles for different surface emissivities in different regimes of convection.

($Ri_L^* = 25$). In each of the three cases, three different surface emissivities ($\varepsilon = 0.05$, 0.45, and 0.85) were chosen. The entire study pertaining to Figure 2 was made for the fixed input comprising $q_v = 10^6\,W/m^3$ and $k_s = 0.25\,W/m\,K$. The figure shows that, for a given surface emissivity (ε), the nondimensional local plate temperature ($\theta(X)$) increases sharply up to a certain distance from the leading edge. Subsequently, it increases mildly and reaches its peak slightly ahead of the trailing edge of the plate. There is a small kink just near the trailing edge of the plate, which may be attributed

to sudden change in the temperature boundary condition just beyond the adiabatic trailing edge of the plate. It may further be seen from the figure that even though there is an expected decrement in local plate temperature with increasing ε in a given regime of convection, the degree of decrement gets more pronounced as Ri_L^* increases from 0.1 to 25. This could be expected because, towards the free convection dominant regime, the inertia forces get completely dominated by the surface emissivity of the plate. Whatever heat dissipation occurs here is predominantly out of radiation and to a very small extent out of buoyancy. Thus, an increase in ε would appreciably decrease local plate temperature here compared to the forced convection dominant regime. In order to quantify the above observations, same calculations were made. It is noticed that, for $Ri_L^* = 0.1$, the temperature of the adiabatic trailing edge of the plate comes down by 17.52% as ε increases from 0.05 to 0.85. Against this, for $Ri_L^* = 1$ and 25 the drops in the temperature of the trailing edge between the same limiting values of ε are, respectively, 29.37% and 43.28%.

Variation of Nondimensional Maximum Plate Temperature with Other Parameters

Figure 3 depicts the nature of variation of nondimensional peak plate temperature (θ_{max}) with reference to surface emissivity (ε) in three different regimes of convection. The study pertains to a fixed input of $q_v = 5 \times 10^5\,W/m^3$ and $k_s = 0.25\,W/m\,K$. Three values of Ri_L^* replicating the three regimes of convection, 25 (free convection), 1 (pure mixed convection), and 0.1 (forced convection), were chosen. Five values of surface emissivity in the range of $0.05 \le \varepsilon \le 0.85$ were considered. The figure shows that, for a given surface emissivity (ε), there is a continuous decrease in θ_{max} as Ri_L^* decreases from 25 to 0.1. In particular, the degree of decrement in θ_{max} with decreasing Ri_L^* is quite substantial at smaller values of ε, while it diminishes towards larger values of ε. This is expected because, for smaller values of ε, the dominant mode of heat dissipation from the plate is convection. Thus, there will obviously be a marked

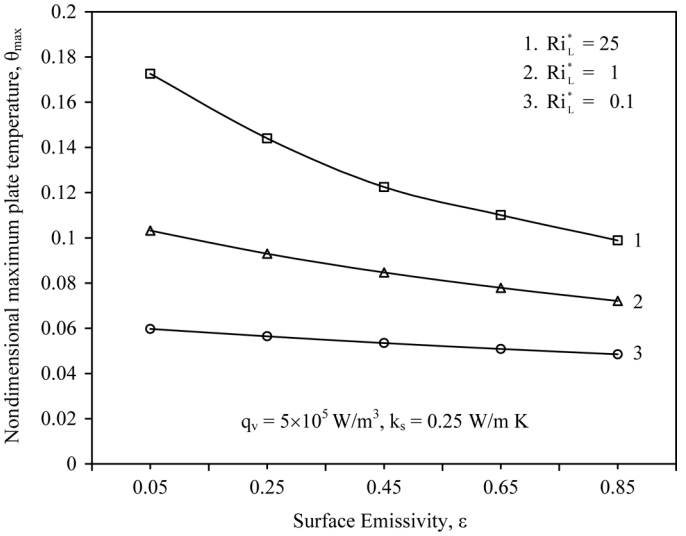

Figure 3. Nondimensional peak plate temperature plotted against surface emissivity for three typical modified Richardson numbers.

effect of Ri_L^* (regime of convection) on peak temperature assumed by the plate at smaller values of ε. For $\varepsilon = 0.85$, on the other hand, since radiation too starts showing its influence on surface heat dissipation, the effect of changing Ri_L^* on θ_{max} is not that substantial. In the present example, θ_{max} decreases by 65.42%, for $\varepsilon = 0.05$, between asymptotic free and forced convection limits. For $\varepsilon = 0.85$, in contrast, θ_{max} decreases by only 50.93% between the same limits of Ri_L^* as above. The figure further shows that θ_{max} decreases progressively as the plate is coated with paints of increasing ε in any given regime of convection. Again here, the above effect is quite substantial in the free convection dominant regime ($Ri_L^* = 25$). This again is due to the dominance of radiation in comparison to convection for larger values of Ri_L^*. In the present example, for $Ri_L^* = 25$, θ_{max} comes down by 42.74% between $\varepsilon = 0.05$ and 0.85. However, for $Ri_L^* = 0.1$, θ_{max} decreases only by 18.76% between the same limits of ε.

Relative Contributions of Mixed Convection and Surface Radiation

Figure 4 shows relative contributions of mixed convection and radiation plotted against surface emissivity (ε) of the plate in three typical regimes of convection ($Ri_L^* = 25$, 1, and 0.1). Five different values of ε were chosen, as shown. It can be seen that, in a given regime of convection, the contribution to heat dissipation from the plate due to mixed convection decreases as ε increases, with a mirror-image increasing trend exhibited by radiation. The above is due to enhanced rate of radiation accompanying increasing ε with other parameters held fixed. The figure further indicates that, for a given ε, the contribution due to radiation increases as one moves from forced to free convection dominant regime. To quantify, in the example considered here, for $Ri_L^* = 25$, convective heat dissipation drops from 93.73% to 51.84% as ε is increased from 0.05 to 0.85. During the above exercise, radiative dissipation shoots up from 6.27% to 48.16%. Also, for $\varepsilon = 0.45$, radiative dissipation is just 11.01% for $Ri_L^* = 0.1$, while it rises to 34.51% for $Ri_L^* = 25$. The figure further

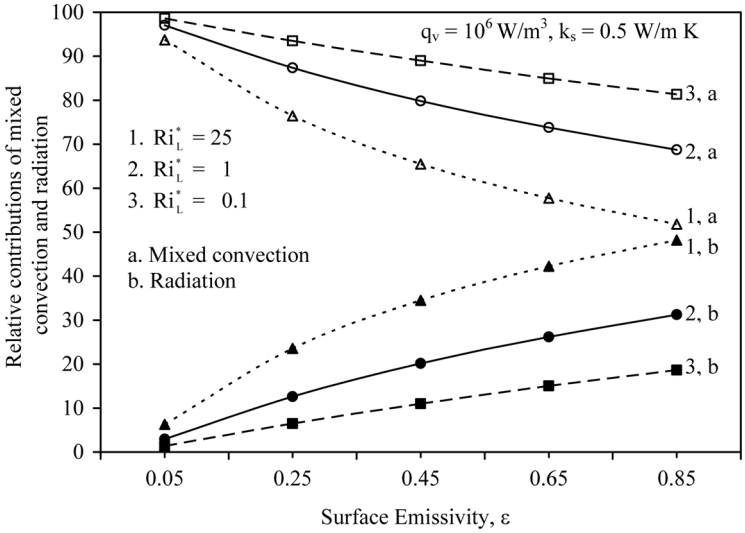

Figure 4. Variation of relative contributions of mixed convection and radiation with surface emissivity in different regimes of convection.

reveals that the share due to radiation in heat dissipation would be as much as 48.16% if the plate is coated with black paint having $\varepsilon = 0.85$. It is also noticed that, if one uses the plate with $k_s = 1\,W/m\,K$ and coats the plate with a paint having $\varepsilon = 0.86$, the contribution from radiation for $Ri_L^* = 25$ would be 50.09%.

Exclusive Role of Surface Radiation

In order to isolate the role surface radiation plays in the present problem, a study of the variation of peak plate temperature (θ_{max}) has been performed without and with radiation taken into reckoning. Figure 5 summarizes the exclusive influence of radiation on peak nondimensional temperature (θ_{max}) assumed by the plate in the entire mixed convection regime ($0.1 \leq Ri_L^* \leq 25$). The study was made for a common input and for seven values of Ri_L^* as shown in the figure. A clear divergence in the two nondimensional peak temperature profiles pertaining to $\varepsilon = 0$ and $\varepsilon = 1$ can be noticed as one moves from $Ri_L^* = 0.1$ to $Ri_L^* = 25$. The above implies that the error that results in θ_{max} calculation by not considering radiation grows with increasing Ri_L^*. This, in turn, unduly overloads the cooling system. It is found that, in the present example, if one ignores radiation, the error in θ_{max} calculation is 40.34% for $Ri_L^* = 0.1$, while it shoots up to 108.53% for $Ri_L^* = 25$.

Study of the Exclusive Effect of Buoyancy

It is known that the present problem pertains to buoyancy-aided mixed convection. It would thus be interesting to isolate the contribution of buoyancy in influencing the peak temperature of the plate. Figure 6 shows the nondimensional maximum plate temperature (θ_{max}) plotted against modified Richardson number (Ri_L^*). This was done to bring out the role of buoyancy in aiding forced convection flow vis-à-vis

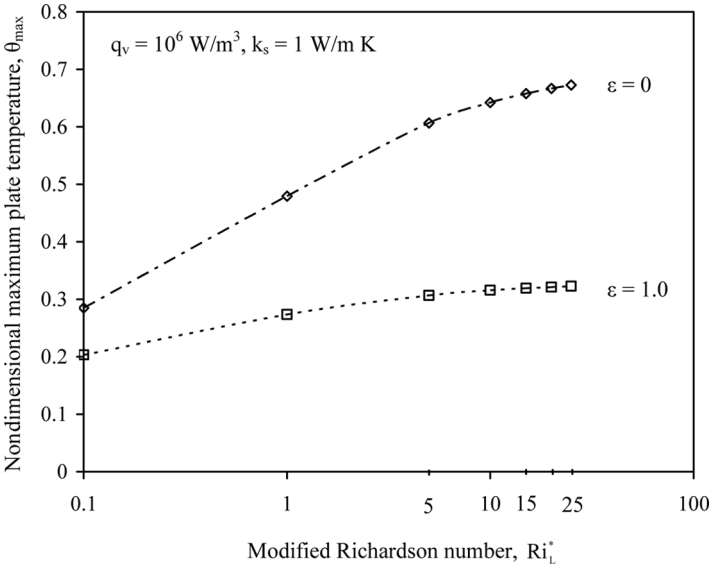

Figure 5. Comparison of nondimensional maximum plate temperatures without and with radiation for various modified Richardson numbers.

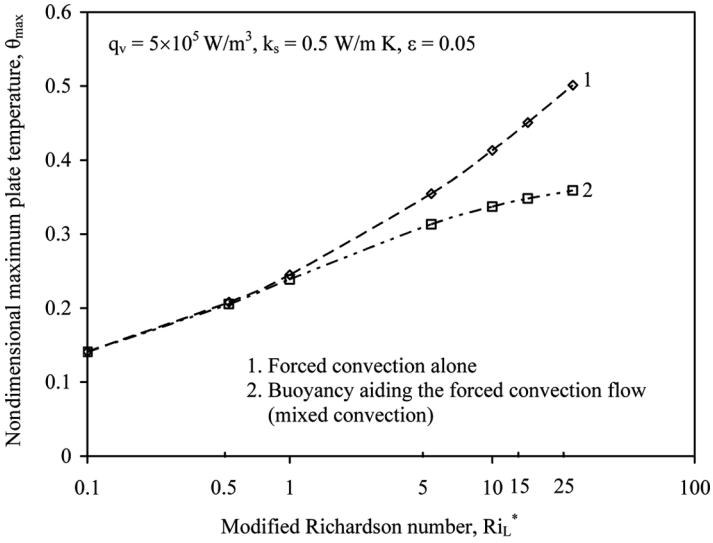

Figure 6. Study of the exclusive effect of buoyancy on nondimensional maximum plate temperature in different regimes of mixed convection.

control of θ_{max} in different regimes of convection. Seven different values were selected for Ri_L^* as shown in the figure, and the study was performed for a fixed set of input parameters ($q_v = 5 \times 10^5\,W/m^3$, $k_s = 0.5\,W/m\,K$, and $\varepsilon = 0.05$). As can be seen, there is hardly anything to choose between (1) non-consideration of buoyancy and (2) consideration of buoyancy up to pure mixed convection ($Ri_L^* = 1$). Beyond $Ri_L^* = 1$, however, there is a well-marked divergence in the two curves pertaining to cases 1 and 2 described as above. Here, buoyancy is clearly helping the impressed (forced convection) flow in bringing down the peak plate temperature (θ_{max}). In the present example, for $Ri_L^* = 1$, buoyancy brings down θ_{max} by only 2.56%. In contrast, in the asymptotic free convection limit of $Ri_L^* = 25$, consideration of buoyancy brings down θ_{max} by 28.39%. The above study clearly highlights the importance of including the buoyancy effect in thermal load calculations, specifically in the range of $1 \le Ri_L^* \le 25$.

Variation of Local Drag Coefficient along the Plate with Other Parameters

Figure 7 shows the local drag coefficient profiles for three typical surface emissivities of the plate ($\varepsilon = 0.05$, 0.45, and 0.85). This was done for given values of q_v, k_s, and Ri_L^* as mentioned in the figure. The figure shows that the local drag coefficient suddenly drops down to a local minimum at the vicinity of the leading edge of the plate. Soon after this, owing to increasing wall velocity gradient, C_{f_x} increases as one moves towards the trailing edge of the plate and reaches a peak at the trailing edge. The above trend is seen for all three surface emissivities chosen. It may further be seen that the value of C_{f_x} decreases, though marginally, with increasing ε. This tells that interaction of surface radiation with convection influences the fluid flow characteristics as well. In the present example, an increase of ε from 0.05 to 0.85 leads to a drop in C_{f_x} by 24.90%.

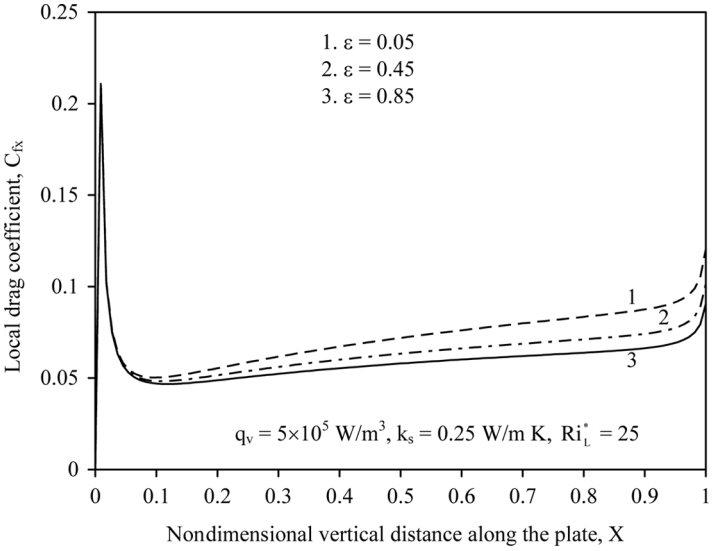

Figure 7. Variation of local drag coefficient along the plate for different surface emissivities.

Figure 8 captures local drag coefficient profiles for five typical values of Ri_L^* encompassing the whole mixed convection regime considered in the present study. The results are obtained for the values of q_v, k_s, and ε fixed as shown. It may be seen that the general trend followed by C_{f_x} along the plate is the same for all values of Ri_L^*. However, there is a continuous increase in C_{f_x} as the flow transits from forced convection dominance to free convection dominance with Ri_L^* increasing from 0.1 to 25. The above is attributed to the additive effect of buoyancy on the induced fluid

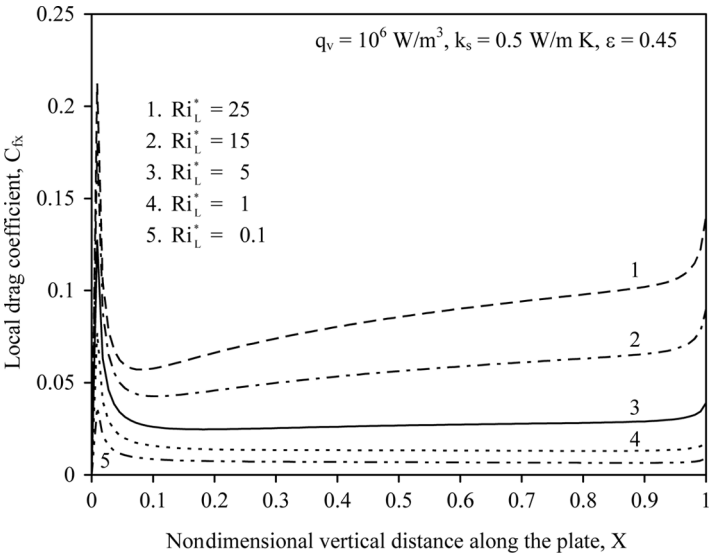

Figure 8. Variation of local drag coefficient along the plate in various regimes of mixed convection.

flow. In the present example, C_{f_x} increases from 0.0087 to 0.1407 at the trailing edge of the plate as Ri_L^* increases from 0.1 to 25.

Variation of Mean Friction Coefficient with Other Parameters

Figure 9 presents mean friction coefficient ($\overline{C}_f$) plotted against emissivity (ε) of the plate for five different values of modified Richardson number (Ri_L^*) encompassing the entire mixed convection regime. The above study is for a given fixed input shown in the figure itself. There is a monotonic decrease in $\overline{C}_f$ with increasing ε for a given Ri_L^*. The only difference is that the degree of decrement in $\overline{C}_f$ with increasing ε diminishes when the operating conditions change from free convection dominance ($Ri_L^* = 25$) to forced convection dominance ($Ri_L^* = 0.1$). The above may be attributed to the decreasing role of surface emissivity in the forced convection environment in comparison to the free convection environment, which results in decreasing effect of ε on mean friction coefficient in such regimes. In the case considered here, $\overline{C}_f$ decreases by 18.07% between $\varepsilon = 0.05$ and $\varepsilon = 0.85$ for $Ri_L^* = 25$. For $Ri_L^* = 0.1$, the same increment in ε (from 0.05 to 0.85) brings down $\overline{C}_f$ by only 0.01%.

The influence of the interaction of mixed convection with internal conduction along the plate on the mean friction coefficient for a given surface emissivity is depicted in Figure 10. This study considers four values of k_s and five values of Ri_L^*, while the values of q_v and ε are fixed, as shown in the figure. The figure shows a linear increase in $\overline{C}_f$ with increasing k_s in any given regime of convection. However, the increment in $\overline{C}_f$ with increasing k_s gets sharper as one moves from $Ri_L^* = 0.1$ to 25. In the present example, $\overline{C}_f$ increases by 45.18% between $k_s = 0.25\,W/m\,K$ and $k_s = 1\,W/m\,K$ for $Ri_L^* = 0.1$. The same increase in k_s as above brings an increase in $\overline{C}_f$ by 211.83% for $Ri_L^* = 25$. These observations substantiate the role of thermal

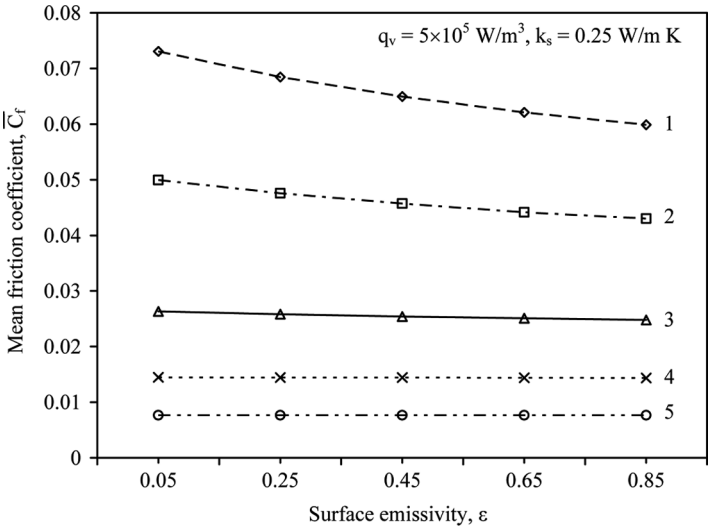

Figure 9. Variation of mean friction coefficient with surface emissivity of the plate in various mixed convection regimes.

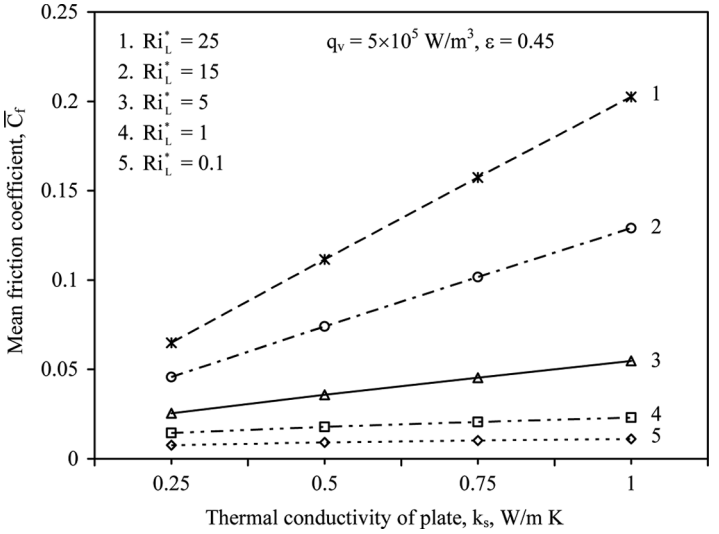

Figure 10. Variation of mean friction coefficient with thermal conductivity of the plate in different regimes of convection.

conductivity in influencing $\overline{C}_f$ more in the free convection dominant regime than in the forced convection dominant regime.

In order to separate the contributions of forced and free convection to the mean friction coefficient, a study has been performed for a fixed input; Figure 11 shows the results thus obtained. Five values of ε were considered and all three regimes of convection were taken up. It may be noted that, for a given ε, the contribution to $\overline{C}_f$ from forced convection drops down as Ri_L^* increases. There is a mirror-image increase in

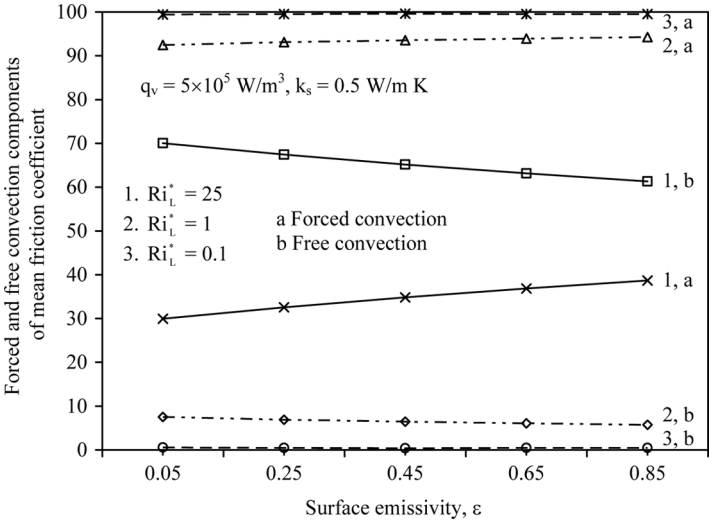

Figure 11. Contributions to mean friction coefficient from forced and free convection plotted with reference to surface emissivity in different regimes of convection.

the contribution of free convection to $\overline{C}_f$. For $Ri_L^* = 0.1$ and 1, there is less than 10% contribution from free convection, with dominance shown by the forced convection component. In contrast, for $Ri_L^* = 25$, which is the free convection limit, the role of forced convection diminishes to less than 40% for all values of ε chosen. Here, as could be physically expected, there is a total dominance by the free convection component in $\overline{C}_f$, which decreases slightly with increasing ε. One can further notice an almost linear variation of the relative contribution of either free or forced convection with surface emissivity. Another feature of the figure is that the forced convection component increases with increasing ε. In summary, it is found that one cannot ignore the effect of buoyancy in the calculation of pumping power in any regime of convection in general and in the free convection dominant regime in particular.

Correlations

Correlations are deduced for nondimensional maximum plate temperature (θ_{max}), nondimensional average plate temperature, (θ_{av}) and mean friction coefficient as functions of various pertinent parameters. For this purpose, a large set of 420 data has been generated from the computer code developed for solving the problem. The correlation for maximum nondimensional plate temperature (θ_{max}) evolved using the above data turned out to be:

$$\theta_{max} = 111.23(1+\varepsilon)^{-0.8}(1+Ri_L^*)^{-0.15}Re_L^{-0.43}\gamma^{-0.91}\left(\frac{N_{RF}}{1+N_{RF}}\right)^{0.04} \tag{10}$$

The above correlation has a correlation coefficient of 0.9948 and an error band of $\pm 0.289\%$. The correlation for average nondimensional plate temperature (θ_{av}) developed making use of the same data as above is:

$$\theta_{av} = 90.62(1+\varepsilon)^{-0.67}(1+Ri_L^*)^{-0.13}Re_L^{-0.44}\gamma^{-0.92}\left(\frac{N_{RF}}{1+N_{RF}}\right)^{-0.05} \tag{11}$$

The above has a correlation coefficient of 0.9947 with maximum deviation limited to $\pm 0.273\%$. A single correlation for mean friction coefficient ($\overline{C}_f$) encompassing the entire mixed convection regime ($0.1 \le Ri_L^* \le 25$) could not be developed with satisfactory error band and correlation coefficient. In view of this, two separate correlations, one for low modified Richardson number range ($0.1 \le Ri_L^* \le 1$) and other for high modified Richardson number range ($1 < Ri_L^* \le 25$), have been deduced. For the range $0.1 \le Ri_L^* \le 1$, the best fit for $\overline{C}_f$ turned out to be:

$$\overline{C}_f = 3.58(1+\varepsilon)^{-0.03}(1+Ri_L^*)^{0.11}Re_L^{-0.54}\gamma^{-0.03}\left(\frac{N_{RF}}{1+N_{RF}}\right)^{-0.04} \tag{12}$$

The above correlation is based on 240 data and has a correlation coefficient of 0.9978 and error band of $\pm 0.122\%$. Likewise, for the range $1 < Ri_L^* \le 25$, the relationship for $\overline{C}_f$ turned out to be:

$$\overline{C}_f = 31.66(1+\varepsilon)^{-0.38}(1+Ri_L^*)^{0.39}Re_L^{-0.74}\gamma^{-0.38}\left(\frac{N_{RF}}{1+N_{RF}}\right)^{-0.38} \tag{13}$$

The above relation, based on 180 data, has a correlation coefficient of 0.9954 and an error band of ±0.506%.

Concluding Remarks

Some of the conclusions from the present study are:

1. The maximum nondimensional plate temperature (θ_{max}), for the given values of q_v and k_s, decreases with increasing emissivity (ε) of the plate in any given regime of convection. However, the degree of decrease of θ_{max} with ε has been found to decrease when the operating condition changes from free convection dominance ($Ri_L^* = 25$) to forced convection dominance ($Ri_L^* = 0.1$).
2. Radiation has been found to assume a significant role in all the regimes of mixed convection. This has been found to be more revealing for higher values of ε. It has been seen that, for $\varepsilon = 0.85$, radiation contributes about 48% to plate heat dissipation for $Ri_L^* = 25$. For the same value of ε, even for $Ri_L^* = 1$ and 0.1, the contributions of radiations are found to be about 32% and 19%, respectively.
3. For a given value of Ri_L^*, in the case of a good reflecting surface ($\varepsilon = 0.05$), convection takes dominance in heat dissipation from the plate, contributing as much as 90 to 95%. Here, expectedly, radiation is insignificant. When a good emitting surface is used, radiation improves its role for the same given value of Ri_L^* as above. Its contribution could range between 18% and 48% depending on the regime of convection (value of Ri_L^*) considered.
4. It has also been seen that, in electronic cooling applications, it would be wise to locate the fan such that buoyancy aids the forced convection flow. Even though not very substantial, a decrement in peak plate temperature and thus the cooling load is noticed when buoyancy-aided mixed convection is considered compared to pure forced convection. This becomes more important when the operating condition is free convection dominant ($Ri_L^* = 25$).
5. The local drag coefficient (C_{f_x}) has been found to drop, though marginally, with increasing ε in a given regime of convection.
6. The local drag coefficient (C_{f_x}) has been found to shoot up with the flow transiting from forced convection dominance to free convection dominance.
7. The mean friction coefficient ($\overline{C}_f$) has been found to increase almost linearly with thermal conductivity of the plate in all regimes of convection. This interactive role of thermal conductivity in influencing $\overline{C}_f$ is noticed to be dominant in the free convection regime ($Ri_L^* = 25$).
8. Useful correlations have been evolved for θ_{max}, θ_{av}, and $\overline{C}_f$ covering a very wide range of governing parameters.

Nomenclature

A_{r1}	geometric ratio, L/t
$\overline{C}_f$	mean friction coefficient
C_{f_x}	local drag coefficient along the plate
Gr_L^*	modified Grashof number, $(g\beta\Delta T_{ref}L^3)/\nu_f^2$
k_f	thermal conductivity of air, W/m K
N_{RF}	radiation-flow interaction parameter, $\sigma T_\infty{}^4/[k_f\Delta T_{ref}/L]$
Pe_L	Peclet number, $Re_L Pr$
Pr	Prandtl number of air

q_v	volumetric heat generation in the plate, W/m^3
Re_L	Reynolds number, $u_\infty L/\nu_f$
Ri_L^*	modified Richardson number, $(g\beta\Delta T_{ref} L)/u_\infty^2$
T	temperature at any location in the computational domain, K or °C
T_∞	free stream temperature of air, K or °C
T_{max}	maximum temperature in the plate, K or °C
T_w	uniform temperature along the plate, K or °C
u, v	vertical and horizontal components of velocity, respectively, m/s
u_∞	velocity of air, m/s
U	nondimensional vertical velocity of air, u/u_∞ or $\partial\psi/\partial Y$
V	nondimensional horizontal velocity of air, v/u_∞ or $[-\partial\psi/\partial X]$
x, y	vertical and horizontal distances, respectively, m
X, Y	nondimensional vertical and horizontal distances, x/L, y/L, respectively

Greek Letters

γ	thermal conductance parameter, $k_f L/k_s t$
θ	nondimensional local temperature, $(T - T_\infty)/\Delta T_{ref}$
θ_{av}	nondimensional average plate temperature
θ_{max}	nondimensional maximum plate temperature
ν_f	kinematic viscosity of air, m^2/s
ξ	buoyancy parameter
ρ, ρ_∞	local and characteristic values of fluid density, respectively, kg/m^3
ψ	nondimensional stream function, $\psi'/u_\infty L$
ψ'	stream function, m^2/s
ω	nondimensional vorticity, $\omega' L/u_\infty$
ω'	vorticity, s^{-1}

Subscripts

cond, x, in	conduction heat transfer into an element along the plate
cond, x, out	conduction heat transfer out of an element along the plate
conv	convection heat transfer from an element
rad	heat transfer by surface radiation from an element

Miscellaneous Symbols

ΔT_{ref}	modified reference temperature difference, $q_v Lt/k_s$, K or °C
Δx_h	height of the plate element chosen for energy balance, m
ΔX_h	nondimensional height of the plate element chosen for energy balance

References

Bejan, A. (1984). *Convection Heat Transfer*, Wiley-Interscience, New York.

Blasius, H. (1908). Grenzschichten in flussigkeiten mit kleiner reibung, *Z. Math. Phys.*, **56**, 1.

Chen, T. S. (1995). Analysis of mixed convection in external flows, in *Proceedings of the Thirteenth National Heat and Mass Transfer Conference, Surathkal, India, December*, 27–36.

Chen, T. S., Armaly, B. F., and Ramachandran, N. (1986). Correlations for laminar mixed convection flows on vertical, inclined and horizontal flat plates, *J. Heat Transfer*, **108**, 835–840.

Gorski, M. A., and Plumb, O. A. (1992). Conjugate heat transfer from an isolated heat source in a plane wall, in *Proceedings of Winter Annual Meeting of the American Society of Mechanical Engineers*, ASME HTD-210, 99–105.

Gosman, A. D., Pun, W. M., Runchal, A. K., Spalding, D. B., and Wolfshtein, M. (1969). *Heat and Mass Transfer in Recirculating Flows*, Academic Press, New York.

Gururaja Rao, C. (2004). Buoyancy-aided mixed convection with conduction and surface radiation from a vertical electronic board with a traversable discrete heat source, *Numer. Heat Transf. Part A Appl.*, **45**, 935–956.

Gururaja Rao, C., Balaji, C., and Venkateshan, S. P. (2000). Numerical study of laminar mixed convection from a vertical plate, *Int. J. Transport Phenomena*, **2**, 143–157.

Gururaja Rao, C., Balaji, C., and Venkateshan, S. P. (2001). Conjugate mixed convection with surface radiation from a vertical plate with a discrete heat source, *J. Heat Transfer*, **123**, 698–702.

Jahangeer, S., Ramis, M. K., and Jilani, G. (2007). Conjugate heat transfer analysis of a heat generating vertical plate, *Int. J. Heat Mass Transfer*, **50**, 85–93.

Kimura, S., Okajima, A., and Kiwata T. (1998). Conjugate natural convection from a vertical heated slab, *Int. J. Heat Mass Transfer*, **41**, 3203–3211.

Kishinami, K., Saito, H., and Suzuki J. (1995). Combined forced and free laminar convective heat transfer from a vertical plate with coupling of discontinuous surface heating, *Int. J. Numer. Methods Heat Fluid Flow*, **5**, 839–851.

Kliegel, J. R. (1959). Laminar free and forced convection heat transfer from a vertical flat plate, Ph.D. diss., University of California, Berkeley.

Lee, S., and Yovanovich, M. M. (1989). Conjugate heat transfer from a vertical plate with discrete heat sources under natural convection, *J. Electron. Packag.*, **111**, 261–267.

Lloyd, J. R., and Sparrow, E. M. (1970). Combined forced and free convection flow on vertical surfaces, *Int. J. Heat Mass Transfer*, **13**, 434–438.

Mendez, F., and Trevino, C. (2000). The conjugate conduction-natural convection heat transfer along a thin vertical plate with nonuniform internal heat generation, *Int. J. Heat Mass Transfer*, **43**, 2739–2748.

Merkin, J. H., and Pop, I. (1996). Conjugate free convection on a vertical surface, *Int. J. Heat Mass Transfer*, **39**, 1527–1534.

Oosthuizen, P. H., and Hart, H. (1973). A numerical study of laminar combined convective flow over a flat plates, *J. Heat Transfer*, **95**, 60–63.

Ostrach, S. (1953). *An Analysis of Laminar Free-Convection Flow and Heat Transfer about a Flat Plate Parallel to the Generating Body Force*, NACA Rep. 1111, U.S. Government Printing Office, Washington, D.C.

Pohlhausen, H. (1921). Der wärmeaustausch zwischen festen körpern und flüssigkeiten mit kleiner wärmeleitung, *Z. Angew. Math. Mech.*, **1**, 115.

Ramachandran, N., Armaly, B. F., and Chen, T. S. (1985). Measurements and predictions of laminar mixed convection flow adjacent to a vertical surface, *J. Heat Transfer*, **107**, 636–641.

Sparrow, E. M., and Gregg, J. L. (1959). Buoyancy effects in forced convection flow and heat transfer, *J. Appl. Mech.*, **81**, 133–134.

Tewari, S. S., and Jaluria, Y. (1990). Mixed convection heat transfer from thermal sources mounted on horizontal and vertical surfaces, *J. Heat Transfer*, **112**, 975–987.

Wang, H. Y., Penot, F., and Sauliner, J. B. (1997). Numerical study of a bouyancy-induced flow along a vertical plate with discretely heated integrated circuit packages, *Int. J. Heat Mass Transfer*, **40**, 1509–1520.

Wilks, G. (1973). Combined forced and free convection flow on vertical surfaces, *Int. J. Heat Mass Transfer*, **16**, 1958–1964.

Zinnes, A. E. (1970). The coupling of conduction with laminar natural convection from a vertical flat plate with arbitrary surface heating, *J. Heat Transfer*, **92**, 528–534.